HEAT TRANSFER CHARACTERISTICS OF MOLTEN SALT FLOWING IN STEAM GENERATOR

by

Shiquan HE[a,b], Linhao WEI[a,b], Jianfeng LU[c*], and Weilong WANG[c]

[a] College of Civil Engineering, Guangzhou University, Guangzhou, China
[b] Guangdong Provincial Key Laboratory Building Energy Efficiency and Application Technology, Guangzhou University, Guangzhou, China
[c] School of Engineering, Sun Yat-sen University, Guangzhou, China

Original scientific paper
https://doi.org/10.2298/TSCI210103225H

The paper respectively investigated the heat transfer characteristics of molten salt flowed in shell-and-tube and double-pipe steam generator. The shell-and-tube steam generator had seven tubes and molten salt flowed outside the tubes, while the double-pipe steam generator had two concentric tubes and molten salt flowed in the annular duct formed by two tubes. Inlet temperature of molten salt ranged from 270 ℃ to 420 ℃. The experimental results showed the effect of temperature on heat transfer coefficient was more significant in the double-pipe steam generator compared to the shell-and-tube steam generator. The heat transfer coefficient firstly increased and then decreased as the increase of temperature. Further numerical study was conducted and the results showed, in the shell-and-tube steam generator, the flow is disturbed by the tube bundle and the boundary-layer near the inner wall is deformed, so the temperature of molten salt cannot obviously affect the heat transfer. In the double-pipe steam generator, an opposite flow was generated in the near cooled wall region by the buoyancy force. When the inlet temperature was below 315 ℃, the velocity of the opposite flow was quite low. In this stage, the heat transfer coefficient increased with the increase of temperature. When the inlet temperature continues to rise to 390 ℃, the opposite flow was enhanced and a stable layer with low velocity formed between the mainstream and the inner cooled wall, resulting increase of heat transfer resistance and impairment of heat transfer coefficient.

Key words: *molten salt, heat transfer characteristics, steam generator, temperature*

Introduction

Molten salt has been widely concerned in nuclear power plants [1, 2] and solar thermal power stations [3, 4] due to the excellent properties [5], such as high working temperature, large thermal capacity, high chemical stability, and being relatively inexpensive, and so on. The high temperature molten salt steam generator [6] is an important heat exchanger and its efficiency affected the performance of the plants or stations. Molten salt in the steam generator is easy to solidify and blocks the flow because of the high melting point [7]. The temperature is also not too high as the molten will decompose [8].

* Corresponding author, e-mail: heshiq@mail2.sysu.edu.cn

Many researchers investigated the heat transfer characteristics of molten salt flow in circular tubes through experiments and simulations. Hoffman [9, 10] experimentally investigated the heat transfer coefficient of ternary salt in a circular tube. Shen [11] experimentally investigated convective heat transfer performances of molten salt in circular tube with non-uniform heat flux and found the Nusselt number on the smooth side with lower heat flux was larger than the value on the side with higher heat flux. Srivastava [12] performed a simulation to analyze the thermal-hydraulic performance of FLiNaK salt in laminar and turbulent regimes. Yang *et al.* [13] analyzed the heat transfer enhancement of a molten salt receiver in the solar power tower. Chen *et al.* [14] experimentally investigated heat transfer characteristics of heat transfer salt in a salt-to-oil concentric tube heat exchanger, and the modified heat transfer correlation was proposed. Yang *et al.* [15] studied the heat transfer characteristics of molten salt flowing in a circular tube with heat flux on a half circumference and found that the heat transfer characteristics were very complex.

However, in some molten salt heat exchanger, molten salt flows outside the tube and the heat transfer characteristics differ from that in the circular tube. Qian *et al.* [16] studied the heat transfer of molten salt through a shell-and-tube molten salt heat exchanger with baffles and found that molten salt seemed to have better heat transfer performance than other working fluids in the baffled shell side. He [17] experimentally studied the heat transfer characteristics of molten salt and water in the same shell-and-tube heat exchanger and pointed out that the heat transfer characteristics of molten salt in the shell side can be predicted through the experimental data of water in the shell side. Actually, the heat transfer characteristics of molten salt in the shell side were related to the structure of the flow channel, and the correlations should be modified by the structural parameters of the flow channel [18-20]. Moreover, the thermal physical properties of molten salt were also of importance in the heat transfer process, especially in a steam generator [21]. Yuan *et al.* [22] experimentally studied thermal performances of a molten salt steam generator and found salt flow rate and temperature affected the overall heat transfer coefficient and energy efficiency through acting on the boiling heat transfer coefficient.

In this paper, the heat transfer characteristics of molten salt at different inlet temperature and the flow rate are investigated in a shell-and-tube steam generator and double-pipe steam generator, respectively. The molten salt flows outside the tube and the water evaporates in the tube. The molten salt flow with a cooled inner wall is studied, and the variable properties are further considered. In addition, a computational model based on the experiments is developed to comprehensively investigate the heat transfer characteristics of molten salt in the two kinds of steam generators.

Experiment study

Experimental set-up

The experimental system mainly included molten salt tank, molten salt pump, steam generator, molten salt flow loop, control system, and acquisition system, which could be referred to [23]. The molten salt in the tank was 1000 kg, and it can be heated to 500 ℃ using electric heaters. Before experiments, the whole molten salt flow loop should be warmed up to above 180 ℃ by electric tracing, and molten salt in the tank was heated to a prescribed temperature. In this article, molten salt was heated to 250-400 ℃ in the tank, and then it was pumped into the steam generator.

The testing sections were a shell-and-tube type and a double-pipe type steam generator, and they were made of stainless steel (304#), as illustrated in fig. 1. The shell-and-tube exchanger without baffle has seven tubes arranged in a staggered triangular pattern with a length of 40 mm. The length of flow channel was 650 mm, and the outer diameter of cylinder shell was 138 mm with a wall thickness of 2.5 mm. The structure parameter of heat transfer tube was Ø 25 × 2.5 mm. The double-pipe exchanger has only one tube, and the distance from inlet to outlet was 1300 mm. The structure parameter of two concentric tubes was Ø 19 × 2 mm and Ø 57 × 2 mm, respectively. In the experiment, high temperature molten salt flowed outside the tube (red region) and feed water (blue region) flowed in the tube. The steam was directly released into the atmosphere, so the steam pressure was 0.1 MPa and the temperature was approximately the boiling point. To decrease heat loss, the steam generator was covered by thermal insulation with a thickness of 100 mm. In this paper, the molten salt heat transfer characteristics were further investigated and the steam discards directly into the atmosphere. In addition, molten salt valves and by-pass channels were used to obtain different flow rates. The molten salt was multi-component salts, and its thermal properties could be referred to tab. 1 [24].

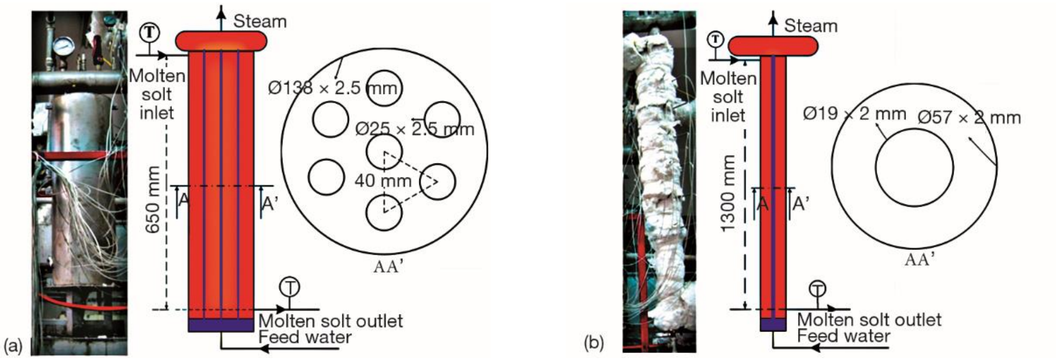

Figure 1. Real imagine and schematic of the steam generator; (a) shell-and-tube steam generator and (b) double-pipe steam generator

Table 1. Thermal properties of molten salt [24]

Properties	Expressions
Density [kgm^{-1}]	P = 2085 – 0.74 T
Heat Capacity [Jkg^{-1}K^{-1}]	c_p = 1549 – 0.15 T
Viscosity, c_P	μ = 31.59 – 0.1948 t + 0.000425t^2 – 0.0000003133 T^3
Thermal conductivity [Wm^{-1}K^{-1}]	λ = 0.697 – 0.000461 T

where T was temperature in °C.

Data processing

The heat flux based on the tube surface was calculated by equation:

$$q = \frac{\rho c_p (T_\text{in} - T_\text{out}) Q_\text{v}}{A} \tag{1}$$

The heat transfer area was determined by:

$$A = n\pi \text{d}l \tag{2}$$

The over heat transfer coefficient of steam generator can be calculated:

$$K = \frac{q}{A\Delta T_{\mathrm{m}}} \tag{3}$$

where T_{in} and T_{out} were the inlet and outlet temperatures of molten salt, Q_{v} – the volumetric flow rate measured by the flow meter, n – the number of tubes, d – the outer diameter of tube, and l – the length of flow channel. The ΔT_{m} was logarithmic mean temperature difference.

In the steam generator, water evaporated in the tube and the boiling heat transfer coefficient was much higher than the coefficient of molten salt in shell side. Therefore, the heat transfer coefficient of molten salt could be obtained according to the Wilson plot method [25]. The flow rate of the water remained unchanged during the experiment, and then the heat transfer coefficient of tube side could be considered as a constant. The over heat transfer coefficient, K, was rewritten as a function of the molten salt velocity, u, shown as:

$$\frac{1}{K} = \frac{1}{h_o} + C_1 \tag{4}$$

$$\frac{1}{h_o} = C_2 \left(\frac{1}{u}\right)^n \tag{5}$$

where C_1, C_2, and h_o were constants, and velocity u could be calculated by volumetric flow rate.

According to and eqs. (4) and (5), the value of constants could be determined though fitting the experimental data, and then the heat transfer coefficient of molten salt, h_{o}, was obtained.

The inlet and outlet temperature of molten salt were measured with 0.3 K uncertainty K-type thermocouples. The flow rate of molten salt was measured by a vortex flowmeter with an uncertainty of 2.5%. The working condition of the experiment was shown in tab. 2. According to the error transfer function [26], the uncertainty of the heat transfer coefficient was 8.96%.

Table 2. Working condition of the experiment

Working condition	Shell-and-tube	Double-pipe
Molten salt flow rate [$\mathrm{m^3h^{-1}}$]	1.0~3.2	0.9~3.3
Molten salt inlet temperature [°C]	270~420	290~420

Experiment results and analyses

Figures 2 and 3 show the heat flux and heat transfer coefficient of molten salt under different temperatures and flow rates. In the figures, Q_{v} is the volume flow rate of molten salt, and T_{in} is the inlet temperature of molten salt. In the shell-and-tube steam generator, the heat transfer coefficient has a little increase when temperature varies from 280 ℃ to 420 ℃. The heat transfer coefficient increases as the increase of volume flow rate. The same phenomenon also can be seen in the double-pipe steam generator. However, the effect of temperature and volume flow rate on the heat transfer coefficient is much more significant in the double-pipe steam generator. When the temperature is around 320 ℃, the heat transfer coefficient at

Q_v = 3 m^3/h is 190% higher than the value at Q_v = 1 m^3/h. Besides, the heat transfer coefficient firstly increases and then decreases when the temperature is higher than 320 °C. The temperature continues to rise to 390 °C, and the coefficient reaches stable. In the double-pipe steam generator, there is only one tube and the molten salt peacefully flowed along the tube surface, whereas the flow of molten salt is strongly disturbed by tube bundle in the shell-and-tube steam generator having seven tubes. Therefore, the effect of temperature and volume flow rate on the heat transfer coefficient is different in the two kinds of steam generators. In order to comprehensively investigate the heat transfer characteristics of molten salt in the steam generator, simulations based on the experiments were further carried out.

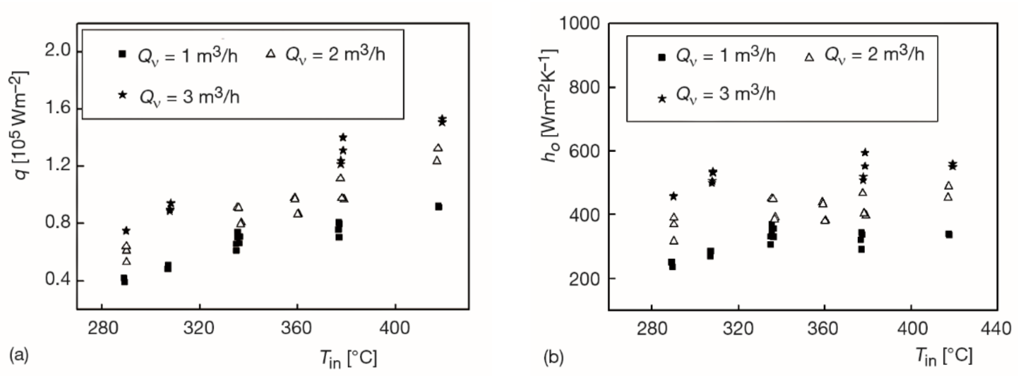

Figure 2. Heat flux and heat transfer coefficient of molten salt in the shell-and-tube steam generator

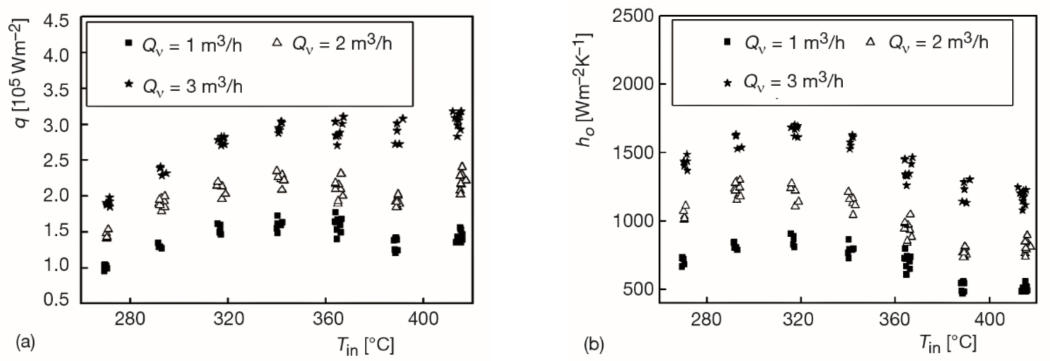

Figure 3. Heat flux and heat transfer coefficient of molten salt in the double-pipe steam generator

Numerical simulation

Governing equations

A 3-D computational domain of the steam generator was built based on the experiment. Steady-state governing equations were used to analyze the heat transfer performance of molten salt in the steam generator. The variable properties were considered due to the large temperature difference in molten salt flow. The governing equations can be written:

$$\frac{\partial(\rho u_j)}{\partial x_j} = 0 \tag{6}$$

$$u_j \frac{\partial}{\partial x_j}(\rho u_i) = \frac{\partial}{\partial x_j}\left[(\mu + \mu_t)\frac{\partial u_i}{\partial x_j}\right] - \frac{\partial P}{\partial x_i} \tag{7}$$

$$u_j \frac{\partial(\rho h)}{\partial x_j} = \frac{\partial}{\partial x_j}\left[\left(\frac{\mu}{\mathrm{Pr}} + \frac{\mu_t}{\sigma_\mathrm{t}}\right)\frac{\partial h}{\partial x_j}\right] \tag{8}$$

where Pr was the molecular Prandtl number, σ_t – the turbulent Prandtl number, and μ_t – the turbulent viscosity. The turbulence equations of kinetic energy and dissipation rate were given:

$$u_j \frac{\partial}{\partial x_j}(\rho k) = \frac{\partial}{\partial x_j}\left[\left(\mu + \frac{\mu_t}{\sigma_k}\right)\frac{\partial k}{\partial x_j}\right] + G - \rho(\varepsilon + D) \tag{9}$$

$$u_j \frac{\partial}{\partial x_j}(\rho \varepsilon) = \frac{\partial}{\partial x_j}\left[\left(\mu + \frac{\mu_t}{\sigma_\varepsilon}\right)\frac{\partial \varepsilon}{\partial x_j}\right] + c_1 f_1 \frac{\varepsilon}{k} G - c_2 f_2 \rho \frac{\varepsilon^2}{k} + E \tag{10}$$

where $c_1 = 1.44$, $c_2 = 1.92$, $\sigma_\mathrm{k} = 1.0$, and $\sigma_\varepsilon = 1.3$ were the constants of the turbulence model [27].

Computational domain and process

To reduce the calculation time, the symmetric boundary was adopted and the domain was half of the experimental value, as illustrated in fig. 4. The inlet condition was given the flow rate and outlet condition was pressure outlet. The tube wall was given the heat flux according to eq. (1). The input data was based on the experimental results, shown in tab. 3. The outer tube wall and the shell wall were adiabatic for double-pipe and shell-and-tube steam generator, respectively. The effect of variable properties of molten salt on heat transfer was considered.

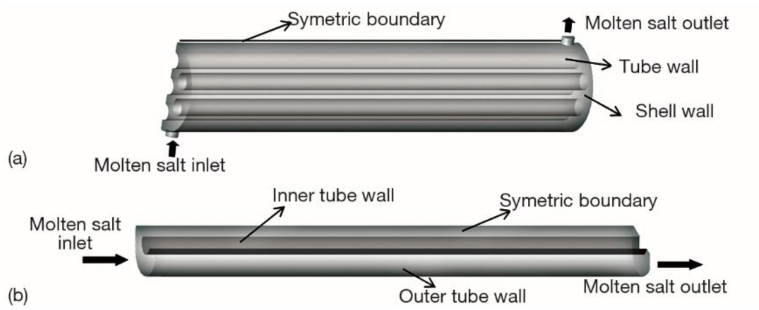

Figure 4. Computational domain of the steam generator

Table 3. Input data of the simulation

Input data	Shell-and-tube	Double-pipe
Molten salt flow rate [$\mathrm{m^3h^{-1}}$]	1.0	1.0
Molten salt inlet temperature [°C]	275/315	270/290/315/340/364/388
Heat flux	eq. (1)	eq. (1)

The domain was carefully meshed to assess the quality of the mesh and structured hexahedral mesh was generated. The mesh element size decreases as it approaches the tube surface to better capture the temperature and velocity gradients in the near-wall region. The mesh detail is provided in fig. 5. Before the calculation, grid independence was conducted through different mesh revolution. In the shell-and-tube steam generator, the mesh with 1374811, 3189117, and 5282014 elements was calculated, and the maximum discrepancies of heat transfer coefficient were 2.1%. In the double-pipe steam generator, three different meshes 1394260, 100800, and 661540 were respectively calculated, and the maximum discrepancies of the flow velocity and heat transfer coefficient were 1.1% and 1.3 %, respectively. Therefore, the mesh with 3189117 and 100800 elements was used for the shell-and-tube steam generator and double-pipe steam generator, respectively.

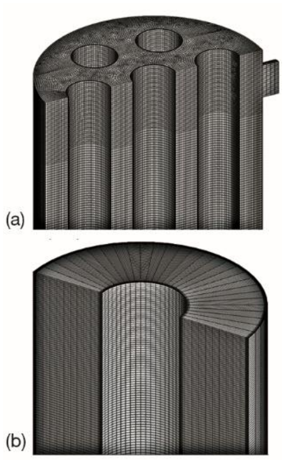

Figure 5. Mesh detail; (a) shell-and-tube steam generator and (b) double-pipe steam generator

All simulations were carried out through the commercial code ANSYS FLUENT 15.0. The double-precision segregated solver was selected. The scheme of pressure-velocity coupling was SIMPLE. The spatial discretization of pressure is PRESTO! The second upwind scheme was used for other control equations. Convergence criteria were set to 10^{-5} for continuity, velocity components and energy.

Model validation

A comparison between the simulation and the experiment is done to validate the numerical results, which is plotted in fig. 6. The open symbols represent the simulation results and the filled square symbols are the experiment results. The error bars are indicated in the simulation results. In the shell-and-tube steam generator, the simulated value is about 11% higher than the experimental measurements. While the discrepancy of outlet temperature between experiment and simulation is about 2.3%. In general, there is an acceptable match between the simulations and the experiments within the considered uncertainty ranges.

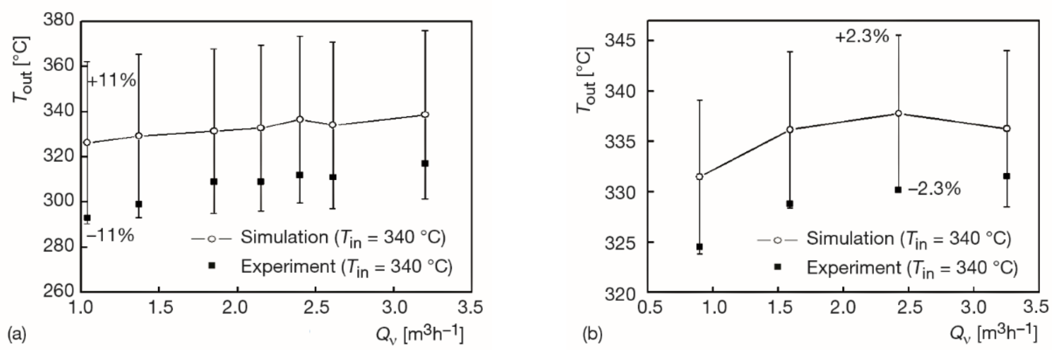

Figure 6. Comparison of outlet temperature between simulation and experimental results; (a) shell-and-tube steam generator and (b) double-pipe steam generator

Simulation results and discussions

Heat transfer characteristics of molten salt flowing in the shell-and-tube steam generator

Figures 7 and 8 show the velocity distribution of molten salt in the shell-and-tube steam generator at the inlet temperature of 275 °C and 315 °C, respectively. The black lines with arrows are the streamlines. Section A is a plane perpendicular to the tube at a distance of 50% of the heat transfer passage. When the molten salt goes into the steam generator, an inlet region forms, and an outlet region can be seen around the outlet as well. Although the volume of the inlet region is larger than the value of the outlet, both regions are a small proportion of the whole passage and so they have little effect on the heat transfer process. According to the streamlines, the molten salt is disturbed by the tube bundle. The velocity distribution in section A is quite in-uniform. Furthermore, the velocity magnitude around a single tube is extremely asymmetric and the velocity near the tube surface is also different from each tube. The velocity distribution changes when the inlet temperature increases from 275 °C to 315 °C, but it is still in-uniform and asymmetric. It means the disturbance is quite strong and it is not obviously influenced by the temperature. Hence, the effect of temperature on flow dynamic performance of shell-and-tube steam generator is not obvious.

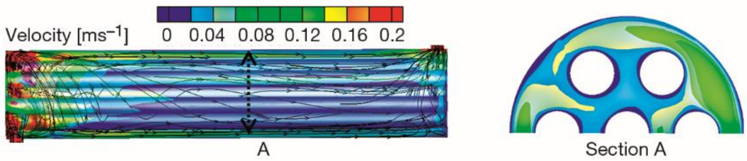

Figure 7. Velocity field of molten salt (T_{in} = 275 °C, Q_v = 1.0 m^3/h)

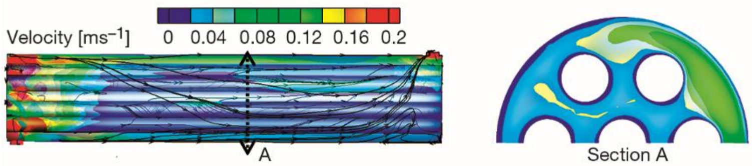

Figure 8. Velocity field of molten salt (T_{in} = 315 °C, Q_v = 1.0 m^3/h)

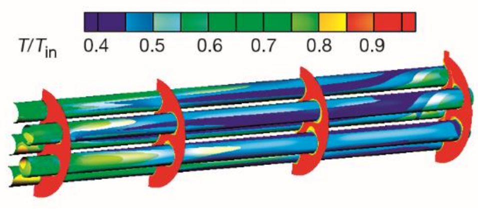

Figure 9. Temperature distribution of molten salt (T_{in} = 275 °C, Q_v = 1.0 m^3/h)

Figure 9 shows the temperature distribution of molten salt in the shell-and-tube steam generator at inlet temperature 275 °C and volume flow rate 1.0 m^3/h. The molten salt flows from the left side to the right side, and four planes perpendicular to the tube are given out. The temperature gradually decreases in the direction of the flow. The cool color on the tube wall suggests a low temperature. The wall temperature is different from tube to tube. Even on a single tube wall, the temperature is in-uniform and the lowest temperature is in the outlet region. This could be attributed to the effect of the tube bundle which has been discussed in fig. 7.

Figure 10 displays the temperature distribution in a plane perpendicular to the tube at a flow distance of $10D_e$. In the shell-and-tube steam generator, the distribution is influenced by the tube bundle, and the temperature boundary-layer on the tube wall is not stable. The boundary-layer is thinned or thickened depending on the flow around the tubes.

Figure 10. Temperature distribution (T_{in} = 275 °C, Q_v = 1.0 m^3/h, L/D_e = 10)

Heat transfer characteristics of molten salt flowing in the double-pipe steam generator

Figure 11 shows the velocity development of molten salt in the double-pipe steam generator at the inlet temperature of 270 °C and 390 °C, respectively. The inner tube wall ($r = r_i$) is the heat transfer surface and the outer tube wall ($r = r_o$) is adiabatic. As can be seen in the figure, the flow is developed when the flow distance is $10D_e$. The velocity distribution is in-uniform. The maximum velocity is nearly at the center of the annular duct and the location of maximum value moves to the outer tube wall as the flow of molten salt. The temperature has a great impact on the flow characteristic. When the inlet temperature increases, the high-velocity region (0.15-0.2 m/s) seems to be squeezed and a movement of maximum location toward the outer tube wall is observed. In addition, the velocity distribution becomes extremely asymmetric when the molten salt flows along the inner tube under the inlet temperature of 390 °C. An interesting phenomenon is observed that the velocity of molten salt attaches to the inner tube wall is negative. In the double-pipe steam generator, the temperature of the inner tube wall is the lowest and the main flow of molten salt is opposite to the direction of gravity. Due to the strong dependence of physical properties on working temperature, the molten salt adjoins the heat transfer surface moves in the opposite direction of the main flow under the impact of gravity.

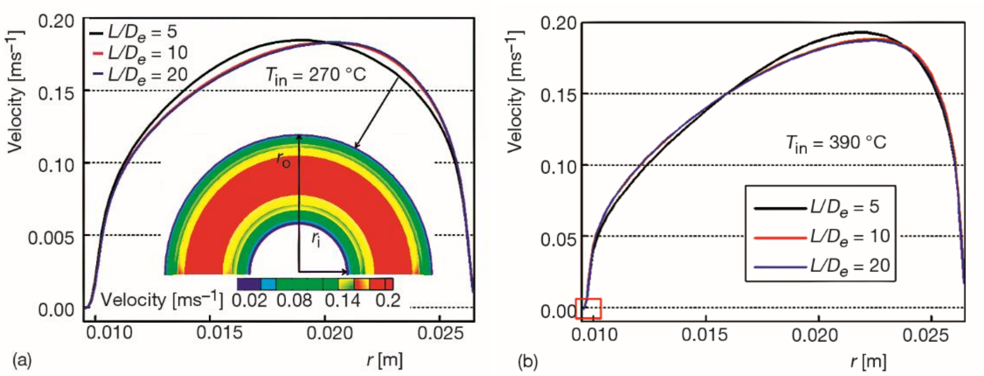

Figure 11. Velocity development of molten salt at different inlet temperature (Q_v = 1.0 m^3/h)

Figure 12 displays the heat transfer coefficient, h_o, and negative velocity of molten salt under different inlet temperatures at a volumetric flow rate of 1.0 m^3/h. When the inlet temperature increases, the heat transfer coefficient firstly increases and then decreases. The

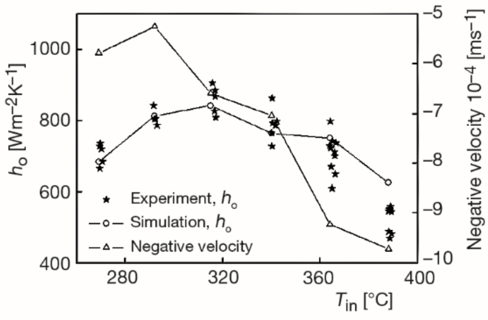

Figure 12. Heat transfer coefficient and negative velocity of molten salt (Q_v = 1.0 m^3/h)

maximum coefficient is about 820 W/m^{2}K at temperature 315 °C. The negative velocity is the velocity of molten salt adhered to the heat transfer surface. According to the figure, although the velocity magnitude is only 10^{-4} m/s, it significantly influences the heat transfer coefficient. The velocity also increases first and then decreases as the increase of inlet temperature. The turning point appears at about 300 °C. When the temperature is less than 300 °C, the opposite flow of molten salt attached to the inner tube wall is not strong enough, and the heat transfer process is still dominated by the mainstream. However, when the temperature is higher than the turning point, the opposite flow is gradually accelerated and impacts the heat transfer process. In this stage, a stable layer with low velocity forms between the mainstream and the inner tube wall. The heat flux cannot efficiently transfer from mainstream to cooled wall when the inlet temperature increases, so the heat transfer coefficient decreases.

To further study the flow characteristics of molten salt in the double-pipe steam generator, fig. 13 plots the turbulent kinetic energy and Reynolds stress at a flow distance of 30D_e under a volumetric flow rate of 1.0 m^3/h. The kinetic energy near the inner tube wall descends as the temperature increases from 270 °C to 390 °C, and the curve at the center (r = 0.014 ~0.02 m) becomes smooth. The Reynolds stress near the inner tube wall also decreases when the inlet temperature rises. The reason could be explained through the mechanism of the opposite flow discussed in fig. 12.

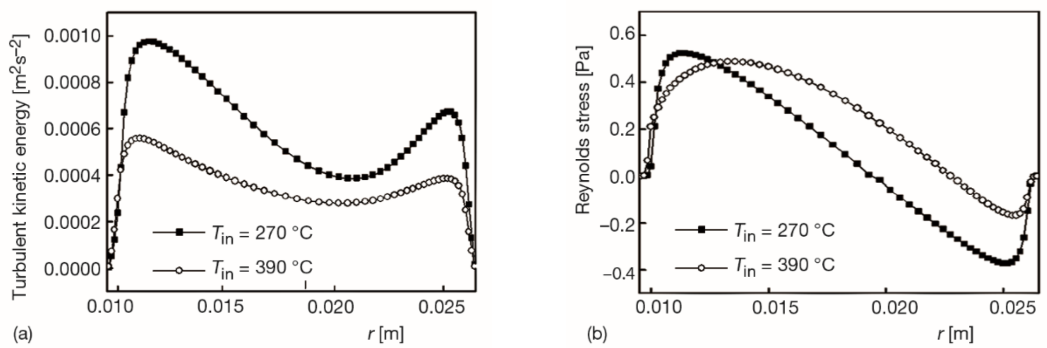

Figure 13. Turbulent kinetic energy and Reynolds stress of molten salt (L/D_e = 30, Q_v = 1.0 m^3/h)

Figure 14 is the plot of temperature and effective thermal conductivity under different inlet temperatures at a volume flow rate of 1.0 m^3/h. As can be seen in the figure, the impact of temperature on the heat transfer characteristics of molten salt was quite significant. According to the temperature plot, when the inlet temperature ranged from 270 °C to 390 °C, the thickness of the temperature boundary-layer was thickened, and the temperature difference enlarged. It means the heat transfer was weakened under higher temperatures. The influence of temperature on effective thermal conductivity is much more visible. The maximum value was reduced by about 7% by 270 °C compared with 390 °C. The effective thermal conductivity near the inner tube wall was also impaired. In the double-pipe steam generator, because of the lack of disturbance generated by the tube bundle, the buoyancy fore induced by the temperature difference [26] significantly influenced the heat transfer characteristics of molten salt. At high inlet temperature, the opposite flow in the near-wall region generated by the buoyancy force was enhanced, and it increased the heat transfer resistant between the main flow and the inner tube wall. Therefore, the heat transfer was impaired and the effective thermal conductivity was reduced.

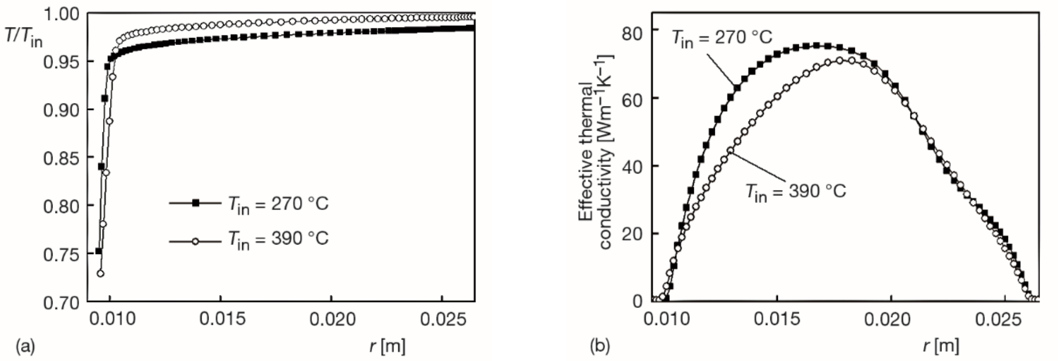

Figure 14. Temperature and effective thermal conductivity of molten salt (L/D_e = 30, Q_v = 1.0 m^3/h)

Conclusion

The paper experimentally and numerically investigated the heat transfer characteristics of molten salt flowing in shell-and-tube steam generator and double-pipe steam generator. According to experimental results, the effect of temperature and volume flow rate on the heat transfer coefficient was more significant in the double-pipe steam generator than that in the shell-and-tube steam generator. Furthermore, in the double-pipe steam generator, the heat transfer coefficient firstly increased and then decreased as the increase of inlet temperature. When the temperature was higher than 390 °C, the change of coefficient was unobvious. The heat transfer characteristic of molten salt was further studied through numerical simulation considering variable properties of molten salt. The results from the simulation agreed that from experiments quite well. In general, the heat transfer characteristics of molten salt flowing in a steam generator were related to the inlet temperature and flow rate. In the shell-and-tube steam generator, the flow was disturbed by the tube bundle and the boundary-layer near the inner wall was deformed, so the temperature of molten salt cannot obviously affect the heat transfer. However, in the double-pipe steam generator, due to the regular flow field, the velocity, as well as the temperature boundary-layer, was affected by the inlet temperature of molten salt, therefore, the influence of temperature was more obvious. An opposite flow of molten salt was found in the near-wall region and it significantly affected the heat transfer characteristics of molten salt.

Acknowledgment

This Project is supported by Guangdong Natural Science Foundation, China (No. 2022A1515010700) and Guangzhou City High School Project (No. 1201581559).

Nomenclature

A – heat transfer area, [m^2]
c_p – specific heat, [Jkg^{-1}K^{-1}]
d – outer diameter of tube, [m]
D – diameter, [m]
D_e – hydraulic diameter, [m]
h – enthalpy, [Jkg^{-1}]
h_o – heat transfer coefficient, [Wm^{-2}K^{-1}]
k – turbulent kinetic energy, [m^{-2}s^{-2}]
K – over heat transfer coefficient, [Wm^{-2}K^{-1}]
l – length of flow channel, [m]
u_i – velocity component in x_i direction [ms^{-1}]
L – length, [m]
P – pressure, [Pa]
Pr – Prandtl number ($=\mu c_p/\lambda$), [–]
q – heat flux, [Wm^{-2}]
Q_v – flow rate, [m^{3}h^{-1}]
r – radius, [m]
Re – Reynolds number ($=\rho u D_e/\mu$) [–]
ΔT_m – logarithmic mean temperature difference [K]
T – temperature [℃]

Greek symbols

μ – dynamic viscosity, [kgm^{-1}s^{-1}]
ρ – fluid density, [kgm^{-3}]
σ_k – k-ε model constant, [–]
ε – turbulent dissipation rate, [m^{-2}s^{-3}]
μ_t – turbulent viscosity, [kgm^{-1}s^{-1}]
σ_t – turbulent Prandtl number, [–]
σ_ε – k-ε model constant, [–]

Subscripts

k – for k-equation
i – inner wall
in – inlet
t – tube wall
ε – for ε-equation
o – outer
out – outlet
v – volume

References

[1] Nagy, K. *et al.*, Steady-State and Dynamic Behavior of a Moderated Molten Salt Reactor, *Annals of Nuclear Energy, 64* (2014), Feb., pp. 365-379
[2] Hathaway, B. J., *et al.*, Demonstration of a Prototype Molten Salt Solar Gasification Reactor, *Solar Energy*, *142* (2017), Jan., pp. 224-230
[3] Zhu, Y., *et al.*, Numerical Study on Heat Transfer Enhancement of Thermal Storage Systems Considering Radiation of Molten Salt, *Solar Energy*, *183* (2019), May, pp. 337-344
[4] Li, Z., *et al.*, Numerical And Experimental Study of Solidification Dangers in a Molten Salt Receiver for Cloudy Conditions, *Solar Energy, 193* (2019), Nov., pp. 118-131
[5] Herrmann, U., *et al.*, Two-Tank Molten Salt Storage for Parabolic Trough Solar Power Plants, *Energy, 29* (2004), 5-6, pp. 883-893
[6] Zavoico, A. B., Solar Power Tower Design Basis Document, Revision 0, Report SAND 2001-2100, Sandia National Laboratories, San Francisco, Cal., USA, 2001
[7] ***, Sandia National Lab., Investigation of thermal storage and steam generator issues, Report SAND 93-7084, Sandia National Laboratories, San Francisco, Cal., USA, 1993
[8] Peng, Q., *et al.*, Thermodynamic Investigation of the Eutectic Mixture of the $LiNO_3$-$NaNO_3$-KNO_3-$Ca(NO_3)(2)$ system, *International Journal of Thermophysics, 38* (2017), 9, pp. 1-10
[9] Hoffman, H. W., Fused Salt Heat Transfer, Part III: Forced Convection Heat Transfer in Circular Tubes Containing the Salt Mixture $NaNO_2$-KNO_3-$NaNO_3$, Report ORNL-2433, Oak Ridge National Laboratory, Oak Ridge, Tenn., USA, 1960
[10] Hoffman, H. W., Fused Salt Heat Transfer, Part II, Forced convection heat transfer in circular tubes containing NaF-KF-LiF eutectic, ReportORNL-1777, Oak Ridge National Laboratory, Oak Ridge, Tenn., USA, 1955
[11] Shen, X. Y., *et al.*, Convective Heat Transfer of Molten Salt in Circular Tube with Nonuniform Heat Flux, *Experimental Thermal and Fluid Science, 55* (2014), May, pp. 6-11
[12] Srivastava, A. K., *et al.*, Heat Transfer and Pressure Drop Characteristics of Molten Salt Fluoride Salt in Circular Pipe, *Apply Thermal Engineering, 61* (2013), 2, pp. 198-205
[13] Yang, M. L., *et al.*, Heat Transfer Enhancement and Performance of the Molten Salt Receiver of a Solar Power Tower, *Apply Energy, 87* (2010), 9, pp. 2808-2811
[14] Chen, Y. S., *et al.*, Convective Heat Transfer Characteristics in the Turbulent Region of Molten Salt in Concentric Tube, *Apply Thermal Engineering, 98* (2016), Apr., pp. 213-219
[15] Yang, X. P., *et al.*, Numerical Simulation Study on The Heat Transfer Characteristics of the Tube Receiver of the Solar Thermal Power Tower, *Apply Energy, 90* (2012), 1, pp. 142-147

[16] Qian, J., *et al.*, Experimental Study for Shell-and-Tube Molten Salt Heat Exchangers, *Apply Thermal Engineering, 124* (2017), Sept., pp. 616-623
[17] He, Y. L., *et al.*, Experimental Investigation on Turbulent Heat Transfer Characteristics of Molten Salt in a Shell-and-Tube Heat Exchanger, *Apply Thermal Engineering, 108* (2016), Sept., pp. 1206-1213
[18] Mavridou, S. G., *et al.*, Experimental Evaluation of Pairs of Inline Tubes of Different Size as Components for Heat Exchanger Tube Bundles, *International Journal of Heat and Mass Transfer, 90* (2015), Nov., pp. 280-290
[19] Rivas, E., *et al.*, Heat Transfer Correlation Between Molten Salts and Helical-Coil Tube Bundle Steam Generator, *International Journal of Heat and Mass Transfer, 98* (2016), Feb., pp. 500-512
[20] Shen, X. Y., *et al.*, Transient Heat Transfer Performance of Molten Salt Tubular Receiver, *Energy Procedia, 158* (2019), Feb., pp. 541-546
[21] He, S. Q., *et al.*, Enhanced Heat Transfer Performances of Molten Salt Mixed Convection in a Vertical Annular Duct, *Heat and Mass Transfer, 50* (2014), 7, pp. 997-1004
[22] Yuan, Y. B., *et al.*, Thermal Performances of Molten Salt Steam Generator, *Apply Thermal Engineering, 105* (2016), July, pp. 163-169
[23] Lu, J. F., *et al.*, Convective Heat Transfer in the Laminar-Turbulent Transition Region of Molten Salt in Annular Passage, *Experimental Thermal and Fluid Science, 51* (2013), 7, pp. 71-73
[24] Peng, Q., *et al.*, The Preparation and Properties of Multi-Component Molten Salts, *Apply Energy, 87* (2010), 9, pp. 2812-2817
[25] Wilson, E. E., A Basis for Rational Design of Heat Transfer Apparatus, *ASME Journal of Heat Transfer, 37* (1915), pp. 47-82
[26] Kline, S. J., *et al.*, Describing Uncertainties in Single Sample Experiments, *Mechanical Engineering, 75* (1953), pp. 3-8
[27] Launder, B. E., *et al.*, Application of the Energy-Dissipation of Turbulence to Calculation of Flow Near a Spinning Disc, *Letters in Heat Mass Transfer, 1* (1974), 2, pp. 131-138

Paper submitted: January 3, 2021
Paper revised: May 11, 2021
Paper accepted: May 18, 2021